Single-Satellite EMI Geolocation via Flexibly Constrained UKF Exploiting Doppler Acceleration

Yanwu Ding, Chaz Minkler, Yimin D. Zhang, Dan Shen, and Khanh Pham

Abstract—Single-satellite geolocation achieves effective localization of ground electromagnetic interference (EMI) signals with a low cost compared to the multi-satellite counterparts. In such systems, the Doppler and Doppler rate are commonly exploited to extract the information of the ground EMI sources and the constrained Unscented Kalman filter (cUKF) is found effective to provide instantaneous EMI locations over time. In this letter, we address the benefit of exploiting Doppler acceleration in the underlying single-satellite geolocation problem, and point out that exploiting additional constraint on the altitude of the ground emitter provides enhanced EMI tracking performance. The importance of such constraint is more pronounced in the beginning of the tracking process, whereas removing such constraint after a short period of time does not compromise the performance. The effect of sampling rates on performance and the required time to converge are investigated.

Index Terms—Electromagnetic interference, single-satellite geolocation, constrained unscented Kalman filter, Doppler frequency, Doppler acceleration

I. INTRODUCTION

The capability of satellites to detect and precisely locate stationary ground electromagnetic interference (EMI) sources holds significant value in space situational awareness and intelligence surveillance. Single-satellite geolocation reduces the operational cost and avoids the needs of synchronization as in multi-satellite systems [1]. Compared to the techniques based on angle-of-arrival estimation [2], [3], Doppler-based methods are simpler and often provide higher accuracy [4]–[6], and thus are widely applied for geolocation using a single satellite [7]–[11]. In [8], the instantaneous frequency is estimated based on the received signal, and the emiiter location is determined by minimizing the difference between the estimated Doppler frequency, which is calculated from the relative geometry between the estimated emitter and known satellite receiver, and that extracted from the received signal. A closed-form solution is obtained in [9] for an initial estimate of the emitter position using the Doppler frequency measurements collected by a single low earth-orbit (LEO) satellite.

Y. Ding and C. Minkler are with the Department of Electrical and Computer Engineering, Wichita State University, Wichita, KS 67260 (emails: yanwu.ding@wichita.edu, cpminkler@shockers.wichita.edu).

Y. D. Zhang is with the Department of Electrical and Computer Engineering, Temple University, Philadelphia, PA, USA (email: ydzhang@temple.edu).

D. Shen and G. Chen are with Intelligent Fusion Technology, Inc. 20271 Goldenrod Lane, Suite 2066 Germantown, MD 20876.

K. Pham is with the Space Vehicles Directorate, Air Force Research Laboratory, Kirtland AFB, NM 87117.

For parametric characterization of the time-varying Doppler frequencies in emitter geolocation exploiting a single satellite, Doppler frequency and Doppler rate are commonly used [4], [12], [13]. The nonlinear properties in Doppler and Doppler rate make the unscented Kalman filter (UKF) a preferred candidate for geolocation because of its superiority in handling high nonlinearity or large uncertainties over the extended Kalman filter (EKF) [14], [15]. Further, the constraint unscented Kalman filter (cUKF) [16] utilizes additional side information to speed up the convergence of emitter geolocation [4], [13]. For example, since the EMI source is known to be on the earth's surface, a constraint is applied for the cUKF in [4] to project the solution space to the earth's ellipsoidal surface. Another constraint is proposed in [13], which ensures that the emitter's altitude is non-negative in the latitude longitude altitude (LLA) coordinate system.

In this letter, we make two important contributions to cUKF-based single-satellite EMI geolocation. First, because the nonlinear Doppler frequencies are generated primarily due to the motion of the satellite with an elliptical orbit, it is importance to account for the Doppler acceleration, which is associated with the satellite jerk, in the underlying problem. This is motivated by the application of jerk motion in the detections for high-maneuvering targets with complex motions [17], [18]. Our second contribution is, because the ground EMI sources have a negligible altitude from the earth surface, adding such constraint to the tracking problem provides additional information to enhance the EMI tracking performance. We point out that the importance of such additional constraint is more pronounced in the beginning of the tracking process, whereas removing such constraint after a short period of time does not compromise the performance. The effect of sampling rates on performance and the required time to converge are investigated. Simulation results are provided to verify the effectiveness of the proposed work.

II. SIGNAL MODEL

We consider the problem of locating a single stationary ground EMI source, located at $\mathbf{p}_e = [x_e, y_e, z_e]^\mathrm{T}$, using a single satellite, flying on its orbit $\mathbf{p}_s(t) = [x_s(t), y_s(t), z_s(t)]^\mathrm{T}$. We denote $\mathbf{r}(t) = \mathbf{p}_s(t) - \mathbf{p}_e$, and its norm $g(t) = \|\mathbf{r}(t)\| = \|\mathbf{p}_s(t) - \mathbf{p}_e\|$ represents the distance between the ground EMI source and the satellite. The signal received by the satellite from the emitter undergoes a Doppler shift brought by the satellite motion, given as [19]

$$f_d(t) = -\frac{f_c}{c} \frac{\mathbf{v}_s^\mathrm{T}(t)\mathbf{r}(t)}{g(t)}, \tag{1}$$

where f_c is the carrier frequency, c is the speed of light, and $\mathbf{v}_s(t)$ is the instantaneous speed of the satellite. The Doppler rate is given as [4]

$$f_r(t) = \frac{\mathrm{d}f_d(t)}{\mathrm{d}t} = -\frac{f_c}{c}\frac{\mathbf{a}_s^T(t)\mathbf{r}(t) + \|\mathbf{v}_s(t)\|^2 - \dot{g}^2(t)}{g(t)}, \quad (2)$$

where $\dot{g}(t) = \mathrm{d}g(t)/\mathrm{d}t$, and $\mathbf{a}_s(t) = \mathrm{d}\mathbf{v}_s(t)/\mathrm{d}t$ is the acceleration of the satellite. Following the steps depicted in the Appendix, the acceleration of the Doppler frequency $f_a(t) = \mathrm{d}f_r(t)/\mathrm{d}t$ is expressed as

$$f_a(t) = \frac{-f_c}{cg(t)}[\dot{\mathbf{a}}_s^T(\mathbf{p}_s(t) - \mathbf{p}_e) + 3\mathbf{a}_s^T(t)\mathbf{v}_s(t) - 3\dot{g}(t)\ddot{g}(t)], \quad (3)$$

where $\ddot{g}(t) = \mathrm{d}\dot{g}(t)/\mathrm{d}t$, and $\dot{\mathbf{a}}_s(t) = \mathrm{d}\mathbf{a}_s(t)/\mathrm{d}t$ is the acceleration rate of the satellite.

III. UKF ALGORITHM WITH FLEXIBLE CONSTRAINTS

A. UKF Algorithm

The basic framework of a Kalman filter associating with the state estimation for a nonlinear dynamic system is given as

$$\mathbf{x}_{k+1} = \mathbf{F}(\mathbf{x}_k) + \mathbf{v}_k, \quad \mathbf{y}_k = \mathbf{H}(\mathbf{x}_k) + \mathbf{n}_k, \quad (4)$$

where k represents the discrete time index, vectors $\mathbf{x}_k \in \mathbb{R}^L$ and $\mathbf{y}_k \in \mathbb{R}^m$ represent the states and measurements, $\mathbf{v}_k \sim \mathcal{N}(\mathbf{0}, \mathbf{Q})$ and $\mathbf{n}_k \sim \mathcal{N}(\mathbf{0}, \mathbf{R})$ are, respectively, the processing and measurement noise vectors. For the geolocalization problem considered, the state vector describes the stationary emitter position with $\mathbf{x}_{k+1} = \mathbf{x}_k$, and the measurement vector contains three components, i.e., Doppler, Doppler rate, and Doppler acceleration. The measurement function $\mathbf{H}(\cdot)$ is nonlinear as described in Eqs. (1)–(3). Compared to [4], [13] where only 2D measurements (Doppler and Doppler rate) are used, we use 3D measurements by adding the Doppler acceleration to account for the high nonlinearity of the Doppler signatures for further performance improvement.

Applying the unscented transformation, the UKF selects a set of sigma points [14], [15]. Let set χ collect $2L+1$ sigma points with corresponding weights w_i for $i = 0, 1, \cdots, 2L$, and $\hat{\mathbf{x}}_k$ is denoted as the kth estimate of $\mathbf{x}$. Given the initial estimate of the state $\hat{\mathbf{x}}_0$ and its covariance matrix $\mathbf{P}_0$, the sigma points at the $(k-1)$th time instant is generated as [20]

$$\chi_{k-1} = [\hat{\mathbf{x}}_{k-1}, \ \hat{\mathbf{x}}_{k-1} + \gamma\sqrt{\mathbf{P}_{k-1}}, \ \hat{\mathbf{x}}_{k-1} - \gamma\sqrt{\mathbf{P}_{k-1}}], \quad (5)$$

where $\gamma = \sqrt{L + \lambda}$, and scaling factor λ controls the spread of the sigma points. The sigma points are then used to predict the state and measurement vectors at the subsequent time-instant as $\chi_{k|k-1}^x = \mathbf{F}(\chi_{k-1})$, $\hat{\mathbf{x}}_k^- = \sum_{i=0}^{2L} w_i^m \chi_{i,k|k-1}^x$, $\mathcal{Y}_{k|k-1} = \mathbf{H}(\chi_{k|k-1}^x)$, and $\hat{\mathbf{y}}_k^- = \sum_{i=0}^{2L} w_i^m \mathcal{Y}_{k|k-1}$. Finally, the measurement is applied to update the mean and covariance matrix of the state. The weights are calculated by $w_0^m = \frac{\lambda}{L+\lambda}$, $w_0^c = \frac{\lambda}{L+\lambda} + (1 - \alpha^2 + \beta)$, $w_i^m = w_i^c = \frac{1}{2(L+\lambda)}, i = 1, \cdots, 2L$, and α and β are the weighting factors.

B. Constrained UKF Algorithm with Flexible Turnoff Time

Considering the fact that the emitter sits on the surface of the earth, the cUKF algorithm in [4] projects the sigma points to the earth's surface by the equation $\frac{x_e^2 + y_e^2}{R_{eq}^2} + \frac{z_e^2}{R_p^2} = 1$, where R_{eq} and R_p are earth's equatorial radius and polar radius, respectively. Another constraint is proposed in [13], where the earth-centered, earth-fixed (ECEF) coordinates $\mathrm{ECEF}(x, y, z)$ are first transformed to the LLA coordinates $\mathrm{LLA}(\mathrm{Lon}, \mathrm{Lat}, \mathrm{Alt})$, and the altitude is set to a nonnegative value as $\mathrm{Alt} = \mu \geq 0$.

In this letter, both constraints are accounted for. However, instead of applying these constraints for the entire duration of UKF implementation, we only enforce the constraint for a short duration at the start of UKF, resulting a cUKF with a flexible time duration of constraints. The constraint period is proper determined to ensure the performance of the UKF is not compromised.

A standard algorithm for cUKF is described in [16]. The flexibly constrained UKF algorithm proposed in this letter is described as bellow:

- Determine the sigma points;
- Apply the above mentioned constraints to the sigma points only for time duration $t \in (0, \tau]$, where τ is a given threshold;
- Predict the state and measurement using the sigma points;
- Apply the UKF algorithm.

Compared to the conventional cUKF, the computational cost is reduced since the constraint is enforced only for a short duration of τ. It is noted that the required time threshold τ depends on the sampling rate.

IV. SIMULATION RESULTS

In the simulations, the emitter tracking performance is evaluated using the root mean square error (RMSE) of the estimated emitter location, defined as

$$\mathrm{RMSE}(k) = \sqrt{\frac{1}{M}\sum_{i=1}^{M} \| \hat{\mathbf{p}}_e(k, i) - \mathbf{p}_e \|^2}, \quad (6)$$

where $\hat{\mathbf{P}}_e(k, i)$ is the estimated position at discrete-time instant k in the ith trial, M is the total number of Monte Carlo trials and is chosen as 800 unless specified otherwise in the simulations. The ground truth of the emitter in the ECEF coordinates is $[x_e, y_e, z_e] = [1902.56, 4828.21, 4008.39]$ km which maps to the LLA coordinate system as [Lon Lat Alt] $= [39.20°, -77.25°, 10 \text{ m}]$. The initial state of the cUKF is set in the ECEF coordinates as $[x_e - 400, y_e + 400, z_e - 50]$ km. The UKF parameters are $\alpha = 0.8, \beta = 2$, and λ is set to -0.184 for 3D measurement and 0.176 for 2D measurement. Suppose accurate satellite position and velocity are available. Doppler, Doppler rate, and Doppler acceleration measurements with Gaussian noise of variances 2.317, 0.0625, and 10^{-4}, respectively, are assumed. The simulations are carried out using the first five (or less) seconds of the measurements. Fig. 1 plots the measurement components for the Doppler, Doppler rate, and Doppler acceleration.

It is noted that, in practice, various factors, such as atmospheric conditions, other interference sources, and satellite
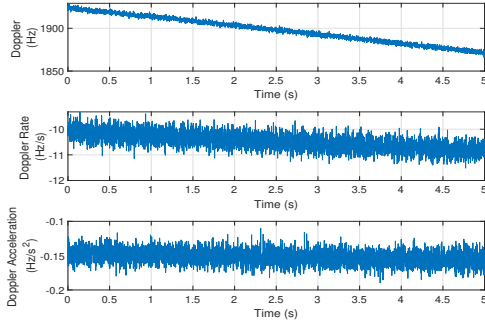
Fig. 1: Measurements for Doppler, Doppler rate, and Doppler acceleration with noise variances of 2.317, 0.0625, and 10^{-4}.
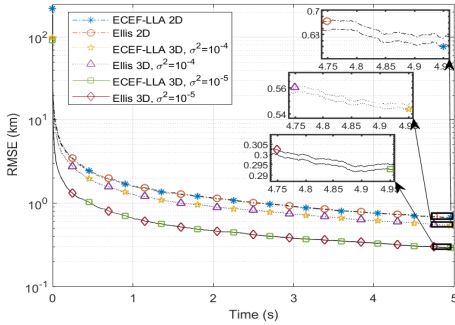

Fig. 3: Performance for different durations on constraint ECEF-LLA with 3D measurements.

Fig. 2: Performance for 2D and 3D measurements.
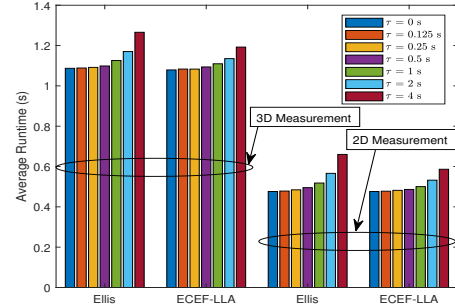
Fig. 4: Averaged runtime with different constraint durations.

hardware inaccuracies, could affect Doppler measurement and EMI localization performance [21], [22]. Such factors are not accounted for in this letter due to the space limitation.

A. Performance improvement using Doppler acceleration

Fig. 2 compares the RMSE performance between those based on 2D (Doppler and Doppler rate) and 3D (Doppler, Doppler rate, and Doppler acceleration) measurements. The sampling rate is $f_s = 1$ kHz. Both constraints proposed in [4] and [13] (with $\mu = 2$) are applied with a full duration of $\tau = 5$ seconds. The RMSE results simulated by the constraints in [4] with 2D and 3D measurements are labeled as "Ellis 2D" and "Ellis 3D", respectively, and those in [13] as "ECEF-LLA 2D" and "ECEF-LLA 3D". For a given dimension size (two or three) of the measurements, as shown in the detail windows in the figure, the performances of the two constraints in [4] and [13] are indistinguishably close. It is evident that, for both constraints, adding the Doppler acceleration as the third measurement assists in state estimation convergence, thus improving the location accuracy. Such an improvement becomes more pronounced when the measurement of Doppler acceleration has higher accuracy with a lower variance of $\sigma^2 = 10^{-5}$.

B. Flexible constrained time period

Fig. 3 shows the RMSE results with the ECEF-LLA constraint exploiting 3D measurements. The sampling rate is $f_s = 1$ kHz. In this figure, the number of trials is $M = 1,500$. The durations of the constraint are, respectively,
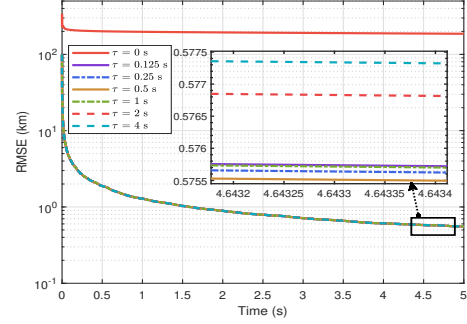
$\tau = 0.125$, 0.25, 0.5, 1, 2, and 4 seconds. For comparison, the performance without constraint is included as $\tau = 0$ seconds. The performance for these different durations on the constraint is very close (within a few meters of difference, as shown in the detailed window). As such, we only need to use a short period of constraint duration to enhance the tracking performance while keeping a low complexity.

It is interesting to note that longer constraint durations with $\tau > 1$ second produce higher RMSE for approximately one meter when the UKF approaches the converging phase. A reason is that the constraint enforces an assumed Alt of $\mu = 2$ m, which may adversely affect the performance since the true height of the emitter is not precisely zero (10 m in this case). Similar observations hold for the constraint in [4].

Using a shorter constrained duration helps save the computational cost. Fig. 4 shows the averaged runtime with respect to M trials for both constraints. The bar-groups for the 3D measurements have higher magnitude than the 2D counterparts. For a given dimension of the measurements (2D or 3D), we have the following observations: i) The averaged runtime increases with longer constraint durations and ii) The constraint in [13] consumes slightly less time than that in [4].

C. Impact of sampling rate

Fig. 5 shows the RMSE for different sampling rates for $f_s = 0.5$, 1, 2, 5, and 10 kHz using 3D measurements under the ECEF-LLA constraint. The duration on the constraint is $\tau = 1$ second. The results show that a higher sampling rate converges faster to a lower estimation error, thus improving the performance. Using five-second measurement data, the RMSE
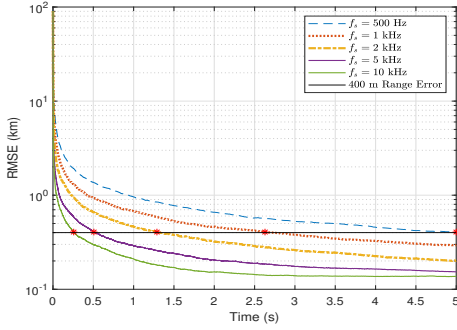
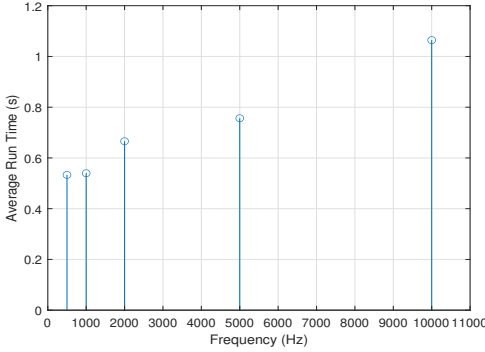Fig. 5: RMSE performance with different sampling rates.

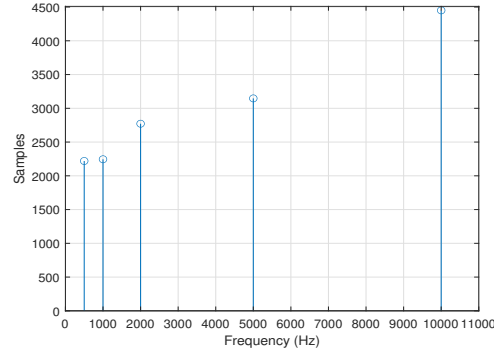Fig. 6: Averaged runtime required to achieve RMSE of 400 m.

Fig. 7: Averaged number of samples required to achieve RMSE of 400 m.

using a laptop with Intel(R) Core i7-10700k CPU @ 3.8 GHz clock and 48 GB RAM. The averaged runtime increases approximately linearly with the sampling rate. For $f_s = 500$ Hz, the runtime is about 0.53 seconds, and that for $f_s = 10$ kHz is 1.06 seconds. Fig. 7 plots the averaged number of samples required for different sampling rates and the results show a similar trend as that in Fig. 6.

V. CONCLUSION

In this letter, we investigated the benefit of Doppler acceleration in the cUKF for EMI geolocation exploiting a single satellite. Flexibility on the duration for the constraint is explored. Without compromising the performance, the time duration to enforce the constraint can be much shorter to save the computational cost. Simulation results also indicate that interpolating the measurements can improve the performance of the cUKF.

APPENDIX
DERIVATION OF DOPPLER ACCELERATION

The range between the satellite and emitter is $g = \|\mathbf{p}_s - \mathbf{p}_e\| = \|\mathbf{r}\|$, where we drop (t) for notation simplicity. The range rate is $\dot{g} = \mathrm{d}g/\mathrm{d}t = \mathbf{v}_s^T \mathbf{r}/g$. The Doppler frequency is

$$f_d = \eta \frac{\mathrm{d}g}{\mathrm{d}t} = \frac{\eta(\mathbf{v}_s - \mathbf{v}_e)^T \mathbf{r}}{g}, \qquad (7)$$

where $\eta = -\frac{f_c}{c}$. The Doppler rate is $f_r = \frac{\mathrm{d}f_d}{\mathrm{d}t} = \eta \frac{\mathrm{d}^2 g}{\mathrm{d}t^2} = \eta \ddot{g}$. Let $\mathbf{a}_s = \dot{\mathbf{v}}_s$ and $\mathbf{a}_e = \dot{\mathbf{v}}_e$. We have

$$\ddot{g} = \frac{1}{g}\frac{d(\mathbf{v}_s^T\mathbf{r})}{dt} - \frac{1}{g^2}\frac{dg}{dt}\mathbf{v}_s^T\mathbf{r} = \frac{1}{g}[\mathbf{a}_s^T\mathbf{r} + \mathbf{v}_s^T\mathbf{v}_s] - \frac{1}{g^2}\dot{g}\mathbf{v}_s^T\mathbf{r}$$
$$= \frac{1}{g}[\mathbf{a}_s^T\mathbf{r} + \mathbf{v}_s^T\mathbf{v}_s - \dot{g}^2] = \frac{A}{g}. \qquad (8)$$

The Doppler acceleration is

$$f_a = \frac{\mathrm{d}f_r}{\mathrm{d}t} = \eta\left(\frac{1}{g}\frac{\mathrm{d}A}{\mathrm{d}t} - \frac{1}{g^2}A\dot{g}\right) = \frac{\eta}{g}\left(\frac{\mathrm{d}A}{\mathrm{d}t} - \dot{g}\ddot{g}\right), \quad (9)$$

where

$$\frac{\mathrm{d}A}{\mathrm{d}t} = \dot{\mathbf{a}}_s^T\mathbf{r} + \mathbf{a}_s^T\mathbf{v}_s + 2\mathbf{a}_s^T\mathbf{v}_s - 2\dot{g}\ddot{g} = \dot{\mathbf{a}}_s^T\mathbf{r} + 3\mathbf{a}_s^T\mathbf{v}_s - 2\dot{g}\ddot{g}. \quad (10)$$

Inserting this into (9), the Doppler acceleration is

$$f_a = \frac{\eta}{g}[(\dot{\mathbf{a}}_s - \dot{\mathbf{a}}_e)^T\mathbf{r} + 3(\mathbf{a}_s - \mathbf{a}_e)^T(\mathbf{v}_s - \mathbf{v}_e) - 2\dot{g}\ddot{g}]. \quad (11)$$

obtained from data with a sampling rate of $f_s = 10$ kHz converges to a floor of about 140 m, whereas that for $f_s = 500$ Hz converges to a floor of about 400 m.

For a given time duration used in the cUKF, longer runtime is expected for a higher sampling rate since it produces more data samples to be processed. To compare the runtime in a reasonably fair manner for different sampling rates, we examine the RMSE at 400 m, which is feasible for the lowest interpolation rate $f_s = 500$ Hz in the figure.

For a given sampling rate, the following steps are applied to obtain the averaged runtime and averaged number of samples:

- For each trial $m = 1, \cdots, M$, run the cUKF using 6 seconds of data with the constraint duration $\tau = 6$ seconds. Here, 6 seconds of data ensure that the RMSE is below 400 m for all sampling rates being considered. In addition, the constraint is applied for the entire duration of the cUKF so that the performance is only affected by the sampling rate.
- For the kth sample, record the runtime $\tau(k, m)$ and the estimate error $e(k, m) = \| \hat{\mathbf{p}}_e(k, m) - \mathbf{p}_e \|$ for $k \geq 1$.
- Backtrack the error to find k_0, such that $e(k_0, m)$ is below 400 m. Backtracking is used to ensure that the error is not higher than 400 m for $k > k_0$.
- Obtain the runtime required to achieve 400 m performance in the mth trial as $t(m) = \sum_{k=1}^{k_0} \tau(k, m)$ and the required number of samples as $S(m) = k_0$.
- Calculate the averaged runtime as $\bar{t} = \sum_{m=1}^{M} t(m)/M$, and the averaged number of required samples as $\bar{S} = \sum_{m=1}^{M} S(m)/M$.

Fig. 6 shows the averaged runtime over 800 trials to achieve the RMSE of 400 m, where the simulations are performed

REFERENCES

[1] J. Mason, "Algebraic two-satellite TOA/FOA position solution on an ellipsoidal earth," *IEEE Transactions on Aerospace and Electronic Systems*, vol. 40, no. 3, pp. 1087–1092, 2004.

[2] C. He, M. Zhang, and F. Guo, "Bias compensation for AOA-geolocation of known altitude target using single satellite," *IEEE Access*, vol. 7, pp. 54 295–54 304, 2019.

[3] E. Williams, C. Bridges, and M. Bowyer, "Nowhere to hide? Passive, non-cooperative maritime surveillance from a nanosat," in *IEEE Aerospace Conf.*, Mar. 2018, pp. 1–10.

[4] P. Ellis, D. V. Rheeden, and F. Dowla, "Use of Doppler and Doppler rate for RF geolocation using a single LEO satellite," *IEEE Access*, vol. 8, pp. 12 907–12 920, 2020.

[5] J. Jensen and R. Bokulic, "Highly accurate, noncoherent technique for spacecraft Doppler tracking," *IEEE Transactions on Aerospace and Electronic Systems*, vol. 35, no. 3, pp. 963–973, 1999.

[6] X. Ning, M. Gui, J. Fang, G. Liu, and Y. Dai, "A novel differential Doppler measurement-aided autonomous celestial navigation method for spacecraft during approach phase," *IEEE Transactions on Aerospace and Electronic Systems*, vol. 53, no. 2, pp. 587–597, 2017.

[7] N. Levanon and E. Weinstein, "Angle-independent doppler velocity measurement," *IEEE Transactions on Aerospace and Electronic Systems*, vol. AES-19, no. 3, pp. 354–359, 1983.

[8] D. Nelson and J. McMahon, "Target location from the estimated instantaneous received frequency," in *Proceedsing of SPIE*, vol. 8020, no. 80200Q, May 2011, pp. 1–8.

[9] N. H. Nguyen and K. Doanay, "Algebraic solution for stationary emitter geolocation by a LEO satellite using Doppler frequency measurements," in *IEEE International Conference on Acoustics, Speech, and Signal Processing (ICASSP)*, 2016, pp. 3341–3345.

[10] H. Witzgall, "A reliable Doppler-based solution for single sensor geolocation," in *Proceedsing of IEEE Aerospace Conference*, 2013, pp. 1–7.

[11] X. Jie, H. Lizhi, M. Zhichao, X. Liang, D. Lian, and Z. Yu, "Methodology on measuring dynamic performance of satellite navigation signal simulator," in *Proceedings of IEEE International Conference on Electronic Measurement & Instruments (ICEMI)*, vol. 03, 2015, pp. 1188–1192.

[12] F. Guo, Y. Fan, Y. Zhou, C. Xhou, and Q. Li, *Space Electronic Reconnaissance: Localization Theories Method*. Wiley, 2014.

[13] D. Shen, G. Chen, and K. Pham, "Passive single satellite geolocation of ground-based EMI sources," in *Proceedings of ION GNSS+*, Oct. 2023, pp. 2384–2394.

[14] S. Julier, J. Uhlmann, and H. Durrant-Whyte, "A new approach for filtering nonlinear systems," in *Proceedsing of American Control Conference*, vol. 3, 1995, pp. 1628–1632.

[15] E. Wan and R. Van Der Merwe, "The unscented Kalman filter for nonlinear estimation," in *Proceedings of IEEE Adaptive Systems for Signal Processing, Communications, and Control Symposium*, 2000, pp. 153–158.

[16] R. Kandepu, L. Imsland, and B. A. Foss, "Constrained state estimation using the unscented Kalman filter," in *Proceedings of Mediterranean Conference on Control and Automation*, 2008, pp. 1453–1458.

[17] J. Wan, Y. Zhou, L. Zhang, and Z. Chen, "A Doppler ambiguity tolerated method for radar sensor maneuvering target focusing and detection," *IEEE Sensors Journal*, vol. 19, no. 16, pp. 6691–6704, 2019.

[18] W. Wu, G. H. Wang, and J. P. Sun, "Polynomial radon-polynomial Fourier transform for near space hypersonic maneuvering target detection," *IEEE Transactions on Aerospace and Electronic Systems*, vol. 54, no. 3, pp. 1306–1322, 2018.

[19] A. Amar and A. J. Weiss, "Localization of narrowband radio emitters based on Doppler frequency shifts," *IEEE Transactions on Signal Processing*, vol. 56, no. 11, pp. 5500–5508, 2008.

[20] R. Van der Merwe and E. Wan, "The square-root unscented Kalman filter for state and parameter-estimation," in *Proceedsing of IEEE International Conference on Acoustics, Speech, and Signal Processing. Proceedings (ICASSP)*, vol. 6, 2001, pp. 3461–3464.

[21] I. Progri, *Geolocation of RF Signals: Principles and Simulations*. Springer, 2011.

[22] D. Shen, G. Chen, Y. Ding, Y. D. Zhang, and K. Pham, "On unscented Kalman filter for NeQuick-G based ionosphere estimation," in *Proceedings of IEEE Aerospace Conference*, 2024, pp. 1–6.